Scientific environment

This thesis was carried out at the Institute of Experimental Medical Research, Oslo University Hospital (IEMR, OUS) as part of the study program "Biological and Medical Physics" at the University of Oslo.

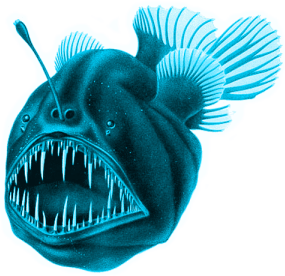

Acknowledgements

Thank someone

(thank medfys for letting me hold a talk at their conference?)

Your Name
Place, Date

Abstract

Background: Heart failure (HF) is a crippling and progressive disease, and the main cause of hospitalization among patients over 65 in Europe (1). Left ventricular (LV) strain measurements can be used as an early indicator of myocardial dysfunction after infarct (2). Previous studies have proven the viability of deriving strain rate tensors from motion-encoded MRI (tissue phase mapping, TPM) to describe the direction and magnitude of strain rate on voxel scale (3), though this method has not yet been implemented to investigate heart dysfunction.

Aim: Our aim was to apply this method to gain new insight on regional myocardial function in rat hearts after myocardial infarction using 3D TPM data of the left ventricle with high spatial/temporal resolution.

Materials & Methods: First, to validate the method, a framework developed in Python was used to reproduce global strain and strain rate curves from 2D short-axis cross-sections of the left ventricle that were compared to literature for established methods (4) (5). The framework was then used to assess the 3D direction of strain rate independently from the conventions of radial, circumferential and longitudinal axes as well as the development of these measurements as a function of days after infarction. The measurements were compared to a sham-operated control group.

Results: Global values calculated using our framework agreed well to the literature. Regional analysis revealed that the strain rate magnitude is reduced in the infarcted area and that this area has reduced strain compared to the other wall sections and the sham control curves. Our data also indicate that the strain rate angles, relative to radial direction from heart center, become less homogenous over time after infarct.

Conclusion: We have shown, for the first time, that strain rate tensor analysis of TPM MRI data is a viable tool to assess regional myocardial strain and strain rate in rat hearts. Our framework also allows for measurement of strain rate directions independently of conventional heart geometry, though the implications of our observations here need further investigation.

Contents

Abbreviations

MRI	Magnetic Resonance Imaging
CMR	Cardiovascular Magnetic Resonance
MI	Myocardial Infarction
EF	Ejection Fraction
LV	Left Ventricle
SHAX	Short Axis
PC-MRI	Phase Contrast MRI
TPM	Tissue Phase Mapping
RF	Radio Frequency
CMR-FT	CMR Feature Tracking

Chapter 1

Introduction

*(cite statements already cited in abstract?)

Mortality for patients with heart failure (HF) is high (6). It is the main cause of hospitalization among patients over 65 years in Europe*, and significantly affects quality of life by impairing social and mental health (7). Further understanding of the disease could lead to ...

HF is characterized by an impairment of the heart's ability to pump blood to the body properly. This can be due to decreased blood supply to the heart muscle tissue (myocardium) or high blood pressure, among other causes (8). Reduced blood supply to specific areas of the myocardium leads to sections of anoxic and necrotic tissue that can't contribute to mechanical pumping work. A parameter to identify reduced myocardial function is ejection fraction (EF), which is the ratio between the amount of blood that flows into the left ventricle (LV) and is pumped out during one cardiac cycle. While a decrease in EF is an accurate indicator of global reduction in function, this parameter is not sensitive to regional changes in function and significant changes in EF tend to occur in the late stages of HF in a majority of cases (9).

It has been shown that regional strain analysis of the myocardium (heart muscle tissue) in the LV can be an early indicator for myocardial dysfunction*, and several different methods using various modalities have been developed for this kind of analysis. Speckle tracking echocardiography (STE) uses naturally occurring speckle patterns in the myocardium seen in ultrasound scans to assess tissue deformation (10). Cardiovascular magnetic resonance (CMR) also plays a large role in regional LV strain analysis. The CMR "tagging" method selectively magnetizes the myocardium in a grid shape at the start of the heart cycle, and follows the relative motion of the grid lines over time to quantify strain (11). CMR feature tracking (CMR-FT) is a post-processing model that tracks the motion of shapes and textures in image sequences from any cine CMR acquisition (12). These methods can be used to determine if a patient is developing heart failure, and whether they could benefit from revascularization therapy (cite).

The methods mentioned above have all been used successfully in clinical application,

but there are certain aspects of their strain analyses that can be done differently. They all assume that myocardial motion occurs within the two-dimensional short-axis (SHAX) plane, which could

*(knowledge gap) (what do the established methods measure? what room for improvement is there?) (what research lays the foundation of thesis? (Selskog / TPM data)) (can strain rate direction tell us something about cardiac function?)

The aim of this thesis is to apply strain rate tensor analysis to study the effects of MI on regional myocardial dysfunction in the LV by applying the Selskog method to MR data of rat hearts. To do this we will first prove that this method is a viable tool to measure cardiac deformation parameters by comparing global strain rate and strain measurements to literature. Different LV segmentation models will be used to look at regional variation in 2D cross-sectional and 3D whole-LV data. We will also make use of the tensor's unique properties to study the direction of strain rate and see if this could lay the foundation of a new myocardial deformation parameter. To study change over time, we will analyze TPM MRI scans of infarcted rat heart LVs and observe how the different measurements progress over weeks after infarct compared to a healthy control group. Using this analysis framework, we will attempt to gain new insight into the dynamics of how myocardial dysfunction develops as the infarcted regions grow.

(subaims: validate selskog method for quantitative analysis of strain using global strain measurements and comparing to literature, use segmentation models to study regional strain variation, study direction of strain rate using tensors, perform statistical analysis to connect deformation measurements to infarct progression)

Chapter 2

Theory

This chapter introduces some fundamental MR theory, heart physiology and the mathematics of strain rate tensor calculation.

2.1 MR theory overview

In this section we will establish a basic theoretical foundation of the physics behind MRI, based on the compendium "Physics of MR imaging" from the FYS4740 course at the University of Oslo (13).

2.1.1 The spin

The most prominent atom in the human body is the hydrogen, found in water molecules and many others. The nucleus of a hydrogen atom is a single proton, and for the sake of simplicity we will imagine the human body as a heterogeneous collection of protons where different tissues have different densities.

In an MRI, a voxel contains signals that are generated from the protons within it. To understand how this signal is produced and measured, it is useful to think of the protons as spinning magnetic dipoles. More precisely, we say that these dipoles "precess" around the static B_0-field from the MRI magnet at the Larmor frequency:

$$\omega_0 = \gamma B_0, \tag{2.1}$$

which is proportional to the B_0 field strength, where γ is the gyromagnetic ratio defined by the material or tissue. We refer to these dipoles as "spins". Other nuclei with an odd number amount of protons also have a spin property, but hydrogen has a higher γ. This makes it easier to detect, which further supports our simplification that living tissue is a collection of protons. The precessing motion is illustrated in Figure 2.1C.

When an object is placed within the magnet it does not initially produce an interpretable

signal. At this point in time, each spin in a voxel precess either parallel or anti-parallel with the $\vec{B}_0$ field direction. Opposite direction spins cancel out, and we end up with a vector sum pointing parallel, which represents the Net magnetization vector $\vec{M}$ as illustrated in Figure 2.1. As long as $\vec{M}$ points parallel to the field, we consider it to be in an equilibrium position. We can generate an MR signal by disturbing this rest state.

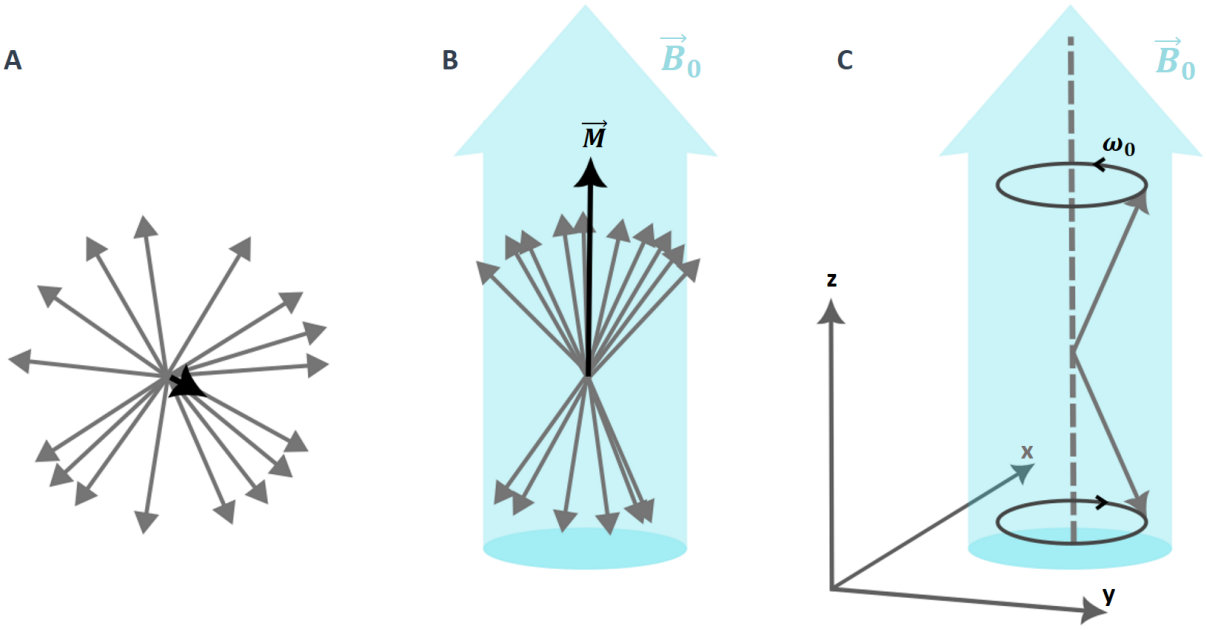

Figure 2.1: ***A:*** *A group of spins pointing in random directions, with no meaningful vector sum.* ***B:*** *The same spins with a magnetic field $\vec{B}_0$ applied, creating a parallel net magnetization vector $\vec{M}$ shown here in its equilibrium position.* ***C:*** *Constituent parallel and anti-parallel spins precessing around $\vec{B}_0$ at the Larmor frequency ω_0.*

2.1.2 RF pulse

Using an orthogonal second field $\vec{B}_1$ to knock $\vec{M}$ out of its equilibrium is what leads us to the signal we need. This field alternates directions at a rate of ω_0 to effectively move $\vec{M}$ without having to overpower the strong $\vec{B}_0$ field. As $\vec{M}$ is moved down at some angle and its composite spins precess in phase, what separates signal from different tissues is how it recovers back to the rest state via two types of "relaxation". $T1$ relaxation is measured by the time it takes for $\vec{M}$ to become parallel to $\vec{B}_0$ again, and $T2$ relaxation depends on the time it takes for the spins to move out of phase again. Figure 2.2 demonstrates how the relaxation of $\vec{M}$ generates a signal that can be measured by a magnetically sensetive reciever coil.

In the figure, $M_\perp(t)$ is the measured transverse component of the MR signal from $\vec{M}$, representing one group of spins with the same Larmor frequency ω_0. In an MRI acquisition, however, the signal will be far more complex because it measures signal from all tissue that is magnetized by the $\vec{B}_1$ field.

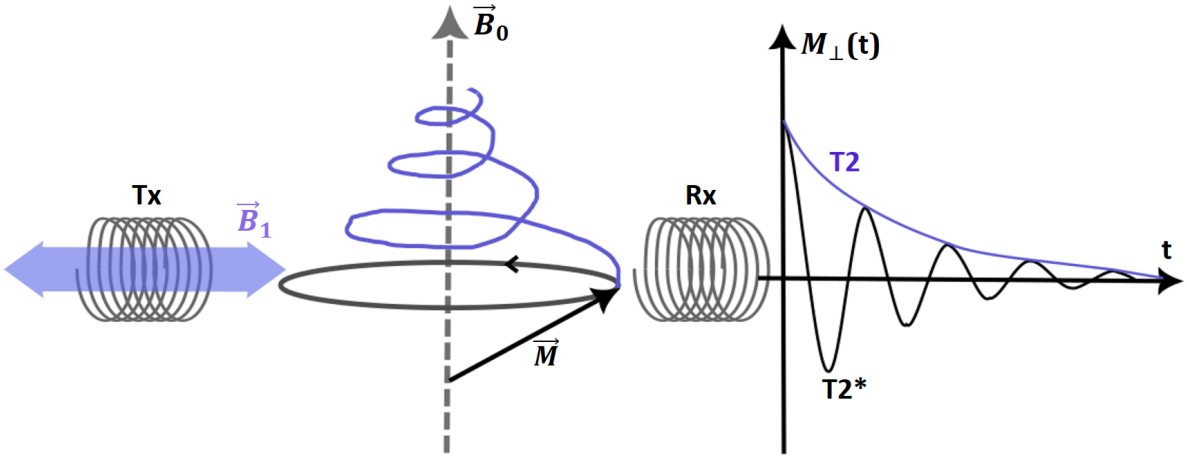

Figure 2.2: A transmitter coil (Tx) creates RF pulses that generates an alternating $\vec{B}_1$ field that moves $\vec{M}$ out of its equilibrium position at some flip angle. The receiver coil (Rx) measures the RF signal generated as the flipped $\vec{M}$ precesses and gradually regains its equilibrium. The orthogonal component $M_\perp(t)$ approaches zero over time as $\vec{M}$ becomes parallel with $\vec{B}_0$ again.

2.1.3 Fourier transform

When interpreting the signal, we are interested in the different frequencies it contains. These tell

To be able to distinguish MR signal frequencies at different positions in a slice, a position dependent Larmor frequency is introduced via a linear gradient $\omega_{local} = \omega_0 + \Delta\omega(r)$ ...

(eddy currents, potential sources of noise in signal?)

2.1.4 K-space

()

2.1.5 Pulse sequences

2.1.6 Motion encoded MRI / PC-MRI

(venc)

2.1.7 MRI geometry

(gantry, isocenter, fase-gradient?)

2.2 Heart physiology

To interpret the data we will be using and the results we get, it is essential to have a fundamental understanding of the heart. We will take a quick dive into anatomy,

physiology as well as look at deformation through strain and strain rate measurements of the LV and what these can tell us about regional myocardial function and HF.

2.2.1 Heart anatomy

Mammal hearts have four chambers that hold and transport blood at different points in the cardiac cycle. The right atrium and right ventricle pump oxygen-poor blood to the lungs, and the left atrium and left ventricle pump oxygenated blood out into the body. This is illustrated in Figure ()*.

*(nice image i am allowed to use)

The chamber walls consist of muscle tissue called the "myocardium", which receive electrical signals that determine heart rate by triggering contracting motions that cause the pumping effect.

2.2.2 Physiology and the cardiac cycle

((Moved from methods, rewrite later) From what we know of LV deformation during the heart cycle, we have some expectations as to how the myocardium should deform. During systole we expect it to compress in the circumferential direction and expand radially during systole as the the heart pumps blood by minimizing the LV cavity. As the heart relaxes and expands again, we expect the opposite. We should be able to observe this from the shapes of the ellipses when plotting over time.)

(what do we mean by 'myocardial function'?)

2.2.3 Myocardial infarction

2.3 Strain and strain rate analysis

This section introduces strain assessment of the heart, some history of the method and different parameters (...)

(strain rate to strain, displacement to strain)

2.4 Strain rate tensor

This section describes how to use velocity gradients to calculate strain rate tensors. Throughout the thesis we will refer to this as the "Selskog method" based on the first author on the article that established the following equations (3).

The n-dimensional velocity gradient tensor ($n \times n$ Jacobian) is calculated like this:

$$L_{ij} = \frac{\partial u_i}{\partial x_j}, \tag{2.2}$$

where u_i, $i = 1,...,n$ are the velocity components in the x_j direction $j = 1,...,n$.

The strain rate tensor is then calculated like this:

$$D_{ij} = \frac{1}{2}\left(\frac{\partial u_i}{\partial x_j} + \frac{\partial u_j}{\partial x_i}\right) = \frac{1}{2}\left(L_{ij} + L_{ij}^T\right). \tag{2.3}$$

The eigenvalues λ_i and eigenvectors $\vec{v}_i$ of D_{ij} are the principal values and the principal directions of strain-rate in the myocardium, as shown in Figure 2.3. The sign of the eigenvalue distinguishes between stretching (positive) and compression (negative) in the direction of the corresponding eigenvector.

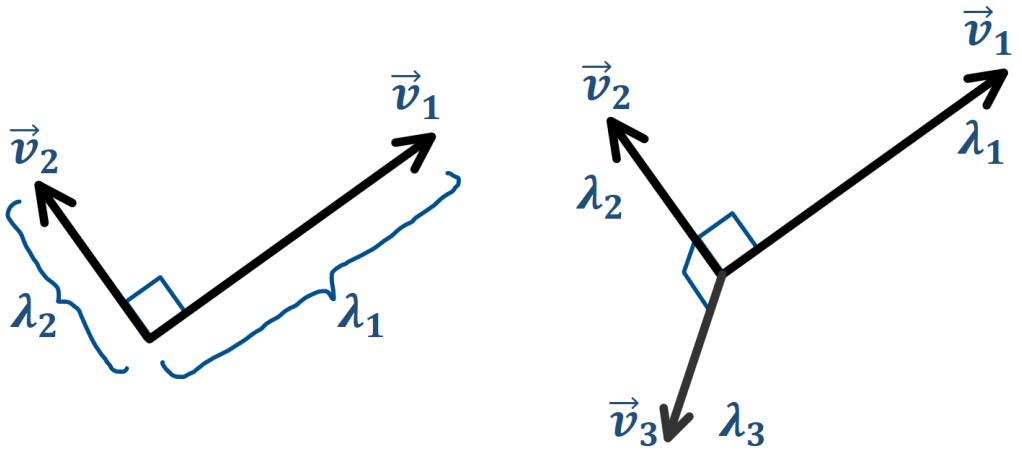

Figure 2.3: Orthogonal eigenvectors $\vec{v}_i$ for a two-dimensional and three-dimensional strain rate tensor D_{ij} (n = 2, n = 3), where the eigenvalues $|\lambda_i|$ represent the vector magnitudes.

The invariant I represents the total amount of strain rate in an n-dimensional strain rate tensor, irrespective of direction:

$$I = \sum_{i=1}^{n} \lambda_i^2. \tag{2.4}$$

Chapter 3

Material & Methods

This chapter will cover the details of the acquisition of our data, LV segmentation models, preparation for analysis and our methods of analysis including the development of our Python framework.

3.1 Data overview

Here we present a short overview of the PC-MRI data that this thesis is based on. All data used was produced by the Sjaastad group at IEMR in 2017-2018, who have already used the same data in a study (23). The specifics are presented mostly the same here, with some adjustments to the study population and acquisition times.

3.1.1 Rat MI model

Male Wistar-Hannover rats (300 g) were anesthetized (96% O2, and 4% isoflurane) and ventilated by endotracheal intubation using a Zoovent ventilator. In ***N*** of the rats, LV MI was induced by proximal ligation of the left coronary artery during maintained anesthesia (98% O2, and 1.5-2.5% isoflurane). The placement of the ligation was deliberately varied to achieve variable infarct sizes. A Sham-operated control group consisting of ***N*** rats underwent the same procedure with the exception of ligation. All experimental protocols were approved by the Norwegian National Animal Research Authority and performed in accordance with the European Directive 2010/63/EU and institutional guidelines (ID 3284).

3.1.2 MRI Acquisition

In time intervals after operation (1, 3, 10, 21 and 42 days), MRI experiments were performed on a 9.4T magnetic resonance system (Agilent Technologies, Inc) using hardware dedicated to rat cardiac imaging. Anesthesia was induced in a chamber using a mixture of O2 and $\approx 4.0\%$ isoflurane and maintained during acquisition in freely breathing animals using O2 and $\approx 1.5\%$ isoflurane. Throughout the examination, ECG, respiration, and body temperature were monitored, the latter maintained at 37.0°C by

heated air. LV short-axis (SHAX) imaging planes were identified from untriggered scout images, and all subsequent acquisitions triggered at the peak of the R wave and gated for respiratory motion. In all data sets, the temporal resolution was equal to the repetition time.

PC-MRI used an RF-spoiled black blood gradient echo cine sequence using 9-point velocity-encoding (22) and rotating field of view (21). Several SHAX slices were aquired to cover the entire LV. All slices were parallel and shared a common center normal. The PC-MRI time series also covered >100% of the heart cycle. Imaging parameters were echo time TE=2.22 to 2.26 ms, repetition time TR=2.93 to 3.21 ms, field of view FOV=50x50 mm, matrix=128x128, slice thickness Δz=1.5 mm, flip angle=7°, velocity encoding strength=13.9 cm/s, signal averaging=2x using rotating field of view, total acquisition time=45 to 50 minutes.

In each PC-MRI slice, the myocardium was segmented using a semiautomatic method that requires the user to delineate the endo- and epicardium at end systole and end diastole. The masks were then automatically propagated throughout the cardiac cycle based on the underlying velocity fields. Lastly, the myocardial masks were divided into 36 equal sectors defined by the LV center. The sectors that were determined to include infarcted tissue during segmenting (LGE MRI?) are noted in the metadata.

3.2 LV segmentation models

To be able to perform regional deformation analysis of the LV, we need to establish models that divide our MRI data into segments that can be measured separately to study variation. Figure 3.1A shows a segmentation model where the LV is divided to study regional variation within a single basal slice. The details of how the slice is segmented is discussed in section 3.3.7. Figure 3.1B shows a second segmentation model consisting of a series of slices covering most of the LV, divided into a basal and apical half. The intention with this model is to use all the processed data to look at regional variation from the base toward the apex.

The "slices" in these models represent masks of the voxels in the TPM scans that contain the LV myocardium, producing quite circular shapes for images in the SHAX plane. These masks cover the LV myocardium, which contains the muscle tissue we will analyze.

((cite?))

(odd nr of slices)

(relation between tensor sampling and these models)

(2d and 3d analysis)

(what does 'global' mean?)

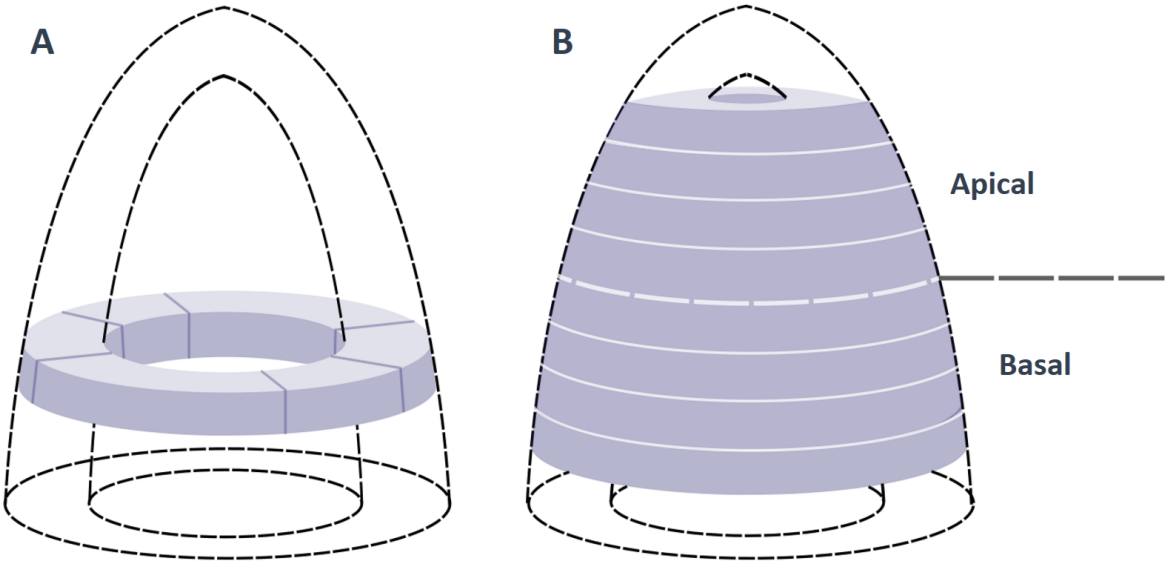

Figure 3.1: The LV segmentation models used in this thesis. ***A****: Model that studies regional variation within one basal slice by segmenting it into separate sections.* ***B****: Model that studies regional variation in a series of slices that covers most of the LV. The stack is split in the middle into an apical and a basal group.*

3.3 Strain rate tensor analysis framework

This section discusses the process of how our Python framework uses the TPM velocity fields to calculate strain rate tensors in the myocardium, visualize them and analyse LV strain rate and strain globally and regionally in the radial, circumferential and longitudinal directions using 2D and 3D strain rate tensors. The framework will also be able to use the tensors to assess the direction of strain rate unrestricted by the conventional axes in heart geometry.

3.3.1 The velocity field

The TPM data is stored as a large MATLAB structure containing many different fields and parameters.

Relevant to this thesis, we have time dependent velocity fields representing cardiac motion, magnitude fields that represent proton density and relaxation dynamics. The structure also contains a binary mask matrix with the same dimensions as the image with value 0 in voxels determined to be outside the myocardium and value 1 inside, which represents a mask designed during processing. Relevant static parameters are infarct sectors for MI hearts with visible infarction, slice position $pss0$ relative to the gantry isocenter and the time points at end systole T_{es} and end diastole T_{ed}.

For our analysis, only tissue in the LV is relevant and we have to exclude noisy signal from the movement of blood. This can be achieved by applying the binary mask to reduce all velocities outside the myocardium to zero.

The velocity field in the myocardium is also affected by noise, so we need to smooth

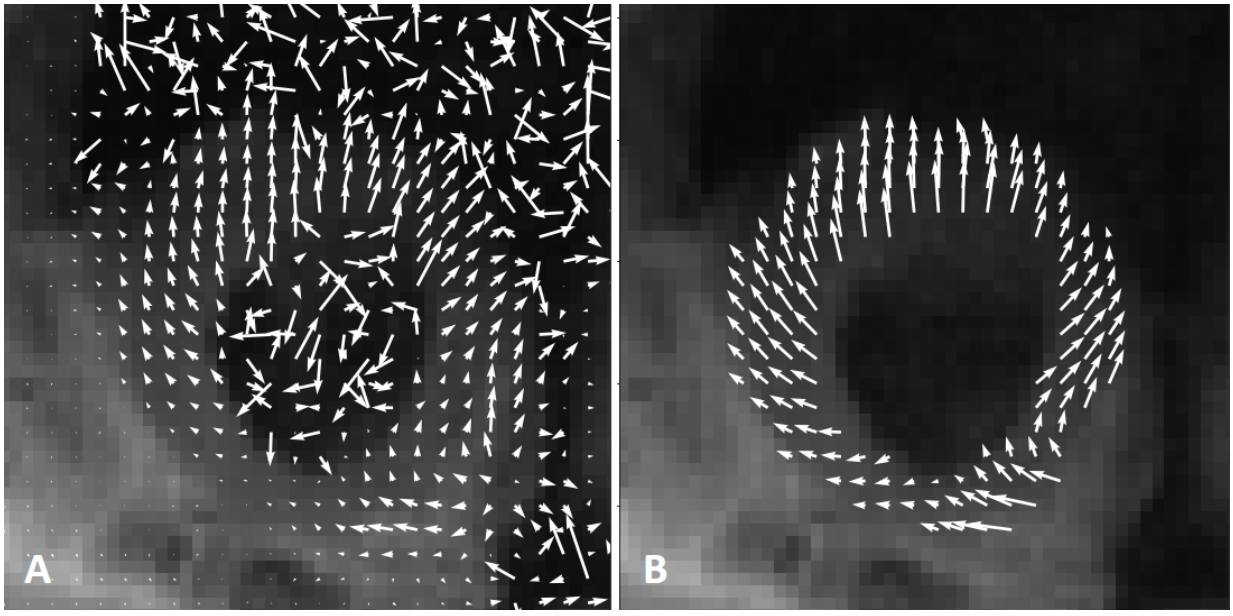

*Figure 3.2: **A**: Velocity field u_i in a 2D SHAX slice in early diastole, including noisy signal in the blood. Magnitude plot in the background. Every other vector is plotted. **B**: The same field at the same frame but with Equation 3.1 applied ($u_{i,smooth}$) and a binary myocardium mask applied.*

the data to compensate for this. For this we can apply the following smoothing function to our velocity field (3):

$$u_{i,smooth} = \frac{(u_i \cdot c) * g}{c * g}, \tag{3.1}$$

where u_i is a velocity field for a spatial component i, and g is a 3D Gaussian function with $\sigma = 2$. Convolution is denoted with a "*". The "c" is defined as a "certainty" matrix, calculated by normalizing the magnitude field to have values in the range $c_k \in [0,\ 1]$ for a voxel k. The intention with the certainty values is to suppress velocity signal from the blood, as it produces lower magnitude values than soft tissue, before smoothing with the Gaussian application function. The "black blood" sequence used to aquire the TPM data further ensures that voxels with blood signal give low certainty values and lesser effect on gradient calculations later.

The effect of smoothing the velocity field and then applying the mask is demonstrated in Figure 3.2. Seeing the effect of the mask is obvious, but notice how the velocity field within the myocardium also becomes more homogenic than in the initial data as well.

3.3.2 Numeric implementation of Selskog method

With the velocity fields from our TPM data we can calculate strain rate tensors in every voxel at every time point via the Selskog method discussed in Section 2.4. This includes smoothing of the velocity fields prior to any calculations to limit the effect of noise on gradient calculations. A numerical implementation of the velocity gradient, weighted by certainty values, is defined like this (3):

$$\frac{\Delta u_k}{\Delta x} = \frac{c_{k+1}(u_{k+1} - u_k) + c_{k-1}(u_k - u_{k-1})}{\Delta x(c_{k+1} + c_{k-1})}, \tag{3.2}$$

where Δx is the resolution in the direction of the gradient and u_k and c_k are the velocity and certainty in the voxel k. To calculate the strain rate tensor D_{ij} (Equation 2.3) in voxel k in a cartesian 3D velocity field, we need this 3×3 gradient tensor L_{ij} via Equation 2.2:

$$L_{ij} = \begin{bmatrix} \frac{\Delta v_x}{\Delta x} & \frac{\Delta v_x}{\Delta y} & \frac{\Delta v_x}{\Delta z} \\ \frac{\Delta v_y}{\Delta x} & \frac{\Delta v_y}{\Delta y} & \frac{\Delta v_y}{\Delta z} \\ \frac{\Delta v_z}{\Delta x} & \frac{\Delta v_z}{\Delta y} & \frac{\Delta v_z}{\Delta z} \end{bmatrix}, \tag{3.3}$$

where the x- and y-directions are in the SHAX plane and the z-direction is orthogonal and out of plane. For a 2×2 gradient tensor from a 2D field, we simply get:

$$L_{ij} = \begin{bmatrix} \frac{\Delta v_x}{\Delta x} & \frac{\Delta v_x}{\Delta y} \\ \frac{\Delta v_y}{\Delta x} & \frac{\Delta v_y}{\Delta y} \end{bmatrix}. \tag{3.4}$$

To get correct gradient values we need to take into account the voxel dimensions in the TPM data, which is especially important in 3D because $\Delta x = \Delta y \neq \Delta z$. From the meta-data we find that the slice thickness is $\Delta z = 1.5mm$, while the in-plane voxel resolution is $\Delta x = \Delta y \approx 0.35mm$.

When we apply masks to the velocity fields we exclude voxels that were determined to be outside the myocardium, but the mask borders may still be an issue when calculating gradients. When the strain rate tensor is calculated in a voxel, the gradients require velocity values in adjacent voxels in the gradient direction (as seen in Equation 3.2). If the voxel is positioned right at the edge, one of its neighbors could be outside the mask and exaggerate the gradient value because it contains noisy signal from the blood.

Noise contamination is supposedly compensated for when using Equation 3.1 to smooth the velocity field, but we can also choose to to exclude the outermost voxels by performing a "binary erosion" of the mask to avoid the issue altogether. This shaves off a layer of voxels on the inside and outside edges and ensures that all in-plane gradient calculations are performed completely within the mask. This is demonstrated in Figure 3.3.

This could, however, mean that we sacrifice data along the epi- and endocardium that is valuable in LV deformation analysis, especially longitudinal strain (24). We will investigate if the smoothing function sufficiently counters border artifacts, and apply binary erosion if not to completely avoid blood signal contamination.

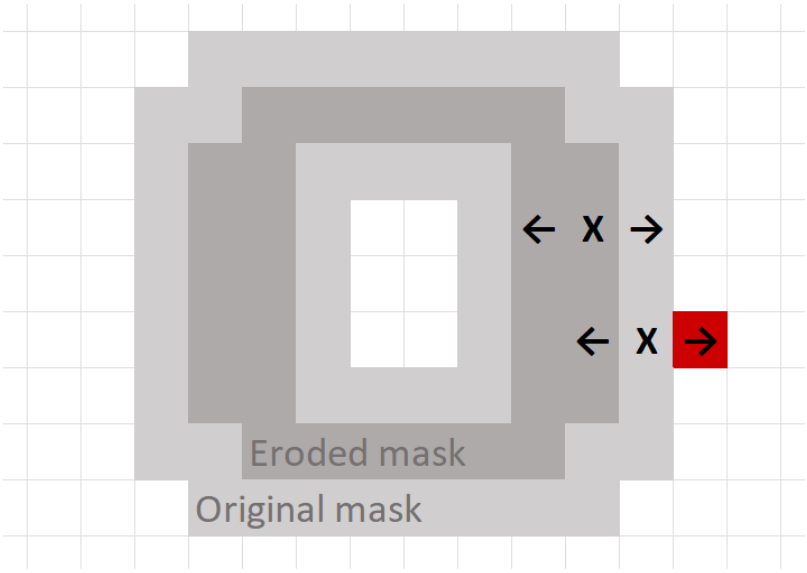

Figure 3.3: A demonstration of binary erosion. For any sampled voxel ("X") in the eroded mask, it will always have neighbors inside the original mask.

Blood signal is especially an issue when calculating gradients in the z-direction. In this case the gradients require velocity values in the slices above and below, and as the radius of the LV masks vary in different positions we hit a lot of zeroes outside the masks. We solve this by applying a "Nearest Neighbor" function, where the framework finds the nearest non-zero value and uses that instead. This leads it to find velocity data in the myocardium nearby.

3.3.3 Ellipsoid tensor visualization

We now have the tools to calculate strain rate tensors in each voxel of the myocardium for every frame over a full heart cycle. To interpret these tensors, it is useful to visualize them in a way that communicates their direction and magnitude of strain rate.

The eigenvectors of the tensor are always orthogonal to each other, and we can use them to span the half-axes of an ellipsoid, or in the two-dimensional case: simply an ellipse. The ellipse shape is intended to deform according to the strain rate direction and magnitude that corresponds to its half-axes, meaning that it should expand along the axis where we have stretching (positive values) and contract along the axis with compression (negative values) or have a roughly spherical shape when the magnitude is around zero. Figure 3.4 illustrates this.

A circular shape could also represent a tensor that either expands or contracts equally along both half-axes. We expect, however, to see compression along one eigenvector and expansion along the other for the majority of 2D strain rate tensors due to the assumption of the heart tissue being incompressible and assuming conservation of mass.

To visualize the tensors as these ellipses, we transform the magnitudes to force the eigenvalues to be positive definite (14). In other words, all positive and negative eigenvalues are transformed to some positive value relative to the unit circle radius of 1.

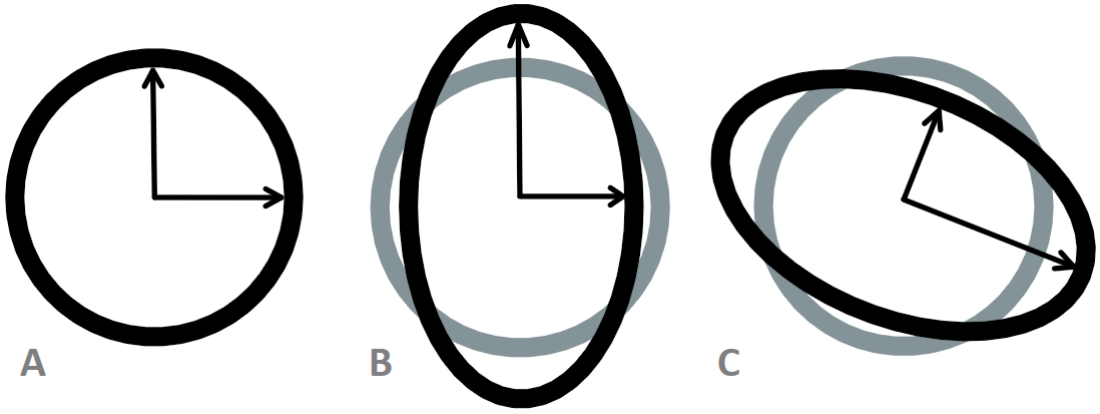

*Figure 3.4: Ellipses spanned by eigenvectors of various magnitudes and directions. **A**: magnitudes around zero; no deformation gives a circular shape. **B**, **C**: Stretch and compression give elliptic shapes.*

We have chosen to use the function $w(\lambda_i) = tanh(\lambda_i) + 1$ where λ_i is some eigenvalue. This transforms the half-axes with positive eigenvalues to have lengths in the range $w \in (1.0,\ 2.0)$, the negative values to have values in the range $w \in (0.0,\ 1.0)$ and ensures that $w(0) = 1$. Letting the eigenvector pairs with transformed lengths $w(\lambda_i)$ span ellipses gives us the desired visuals in Figure 3.4.

Keep in mind that this function is only applied as a *visual* tool for the ellipse plotting, and not in the quantitative analysis. This means that the constants above are somewhat arbitrary and could be scaled later for visibility, but the point is that it produces the correct ellipse proportions and normalizes the scale to make the low magnitude tensors clearly visible. The same principle goes for 3D strain rate tensors too, but with an ellipsoid spanned by three orthogonal eigenvectors.

To more effectively communicate the regional variation in strain rate direction and magnitude visually, we can choose different parameters to assign to a color range and to the opacity of the ellipses. One such parameter, from assessing the direction of some tensor in the myocardium, is the angle θ_i of the eigenvectors relative to radial direction as demonstrated in Figure 3.5.

Here we also demonstrate that the alignment of the ellipse relative to the radial and circumferential (tangential) axes determines strain rate direction. In other words, if you flip any of the eigenvectors 180° they still correctly describe the direction. Because the LV moves and deforms from its initial position and shape, we need to calculate the LV center position for every frame to ensure that this geometric model is consistent.

This means that all possible ellipse alignments in xy-space can be described by the range of a single angle $\theta_1 \in [0,\ 90]°$, where 0° represents a completely radial alignment and 90° a circumferential alignment. θ_2 is always orthogonal to θ_1 in the xy-plane for 2D strain rate tensors. We will map the angle of each tensor's most positive strain rate (stretch) to a color scale with this range to get a visual of directional homogeneity when plotting the ellipses. The opacity will be assigned to the Invariant I, representing total strain rate magnitude, via Equation 2.4.

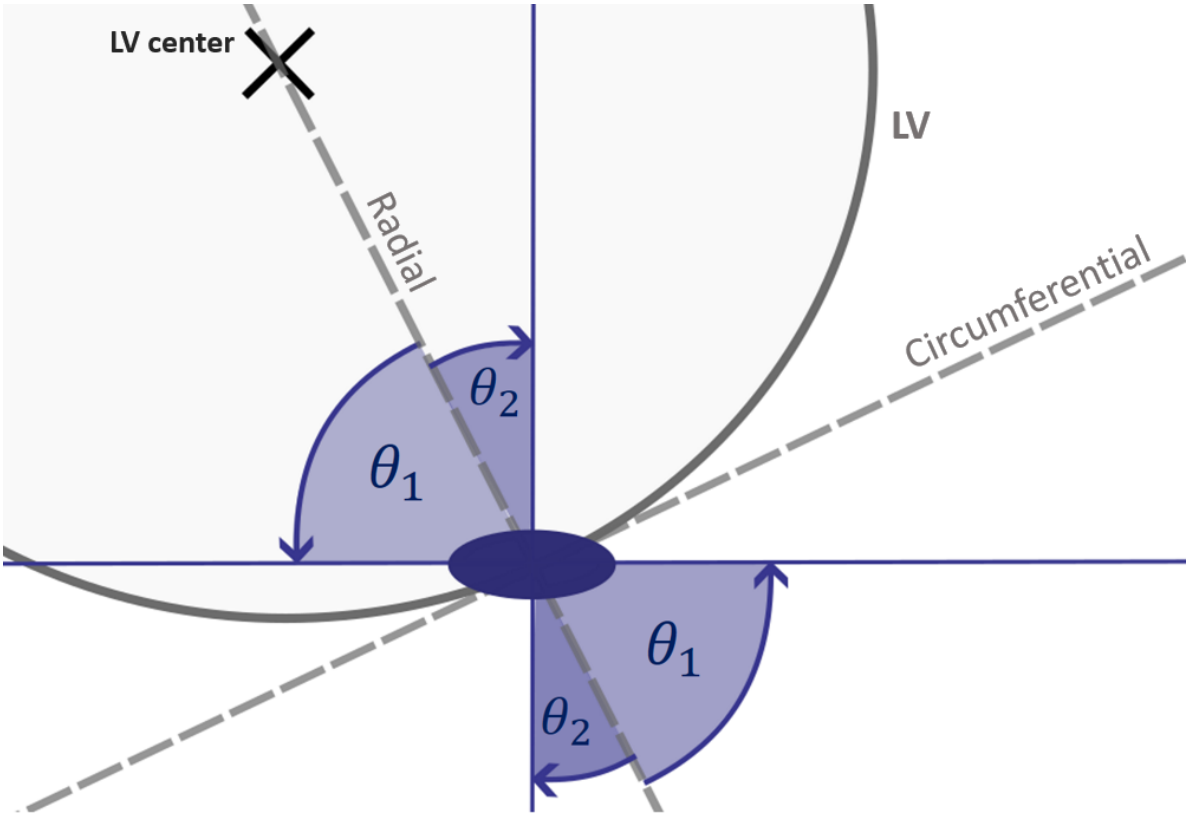

Figure 3.5: Diagram of an ellipse positioned in a coordinate system with radial and circumferential axes (dashed lines) defined by LV geometry and ellipse position. The ellipse half-axes, representing the tensor eigenvectors $\vec{v}_1$ and $\vec{v}_2$, are oriented with angles θ_1 and θ_2 with respect to the radial axis.

3.3.4 Eigenvector decomposition

The angles θ_i will not only be used for visual analysis, but will also be used to gather quantitative information. Vector decomposition, using the eigenvector angles θ_i and eigenvalues λ_i as vector length, can be used to find the radial and circumferential components r_i and c_i of the strain rate tensors. These components are simple to find using the trigonometric formulas for right triangles, which we can construct with the eigenvalue λ_i as the hypotenuse and r_i and c_i as the catheti. This is shown in Figure 3.6.

For a slice at some time-point in our MR recording we generally have hundreds of voxels in the LV to sample, so we need some way of organizing the data we collect from the tensors in each of these. When using 2D strain rate tensors to analyze the voxels in the LV mask we are interested in their weighted average sum of radial and circumferential strain rate where the radial and circumferential components r_i and c_i of one tensor are calculated as shown in Figure 3.6. The weighted average sums of these components represent the global radial and circumferential strain rate for this LV slice.

3.3.5 Global LV strain rate

When plotting the global radial and circumferential strain rate for all of the time-points of velocity data in the whole LV, we expect to see curves resembling the global strain

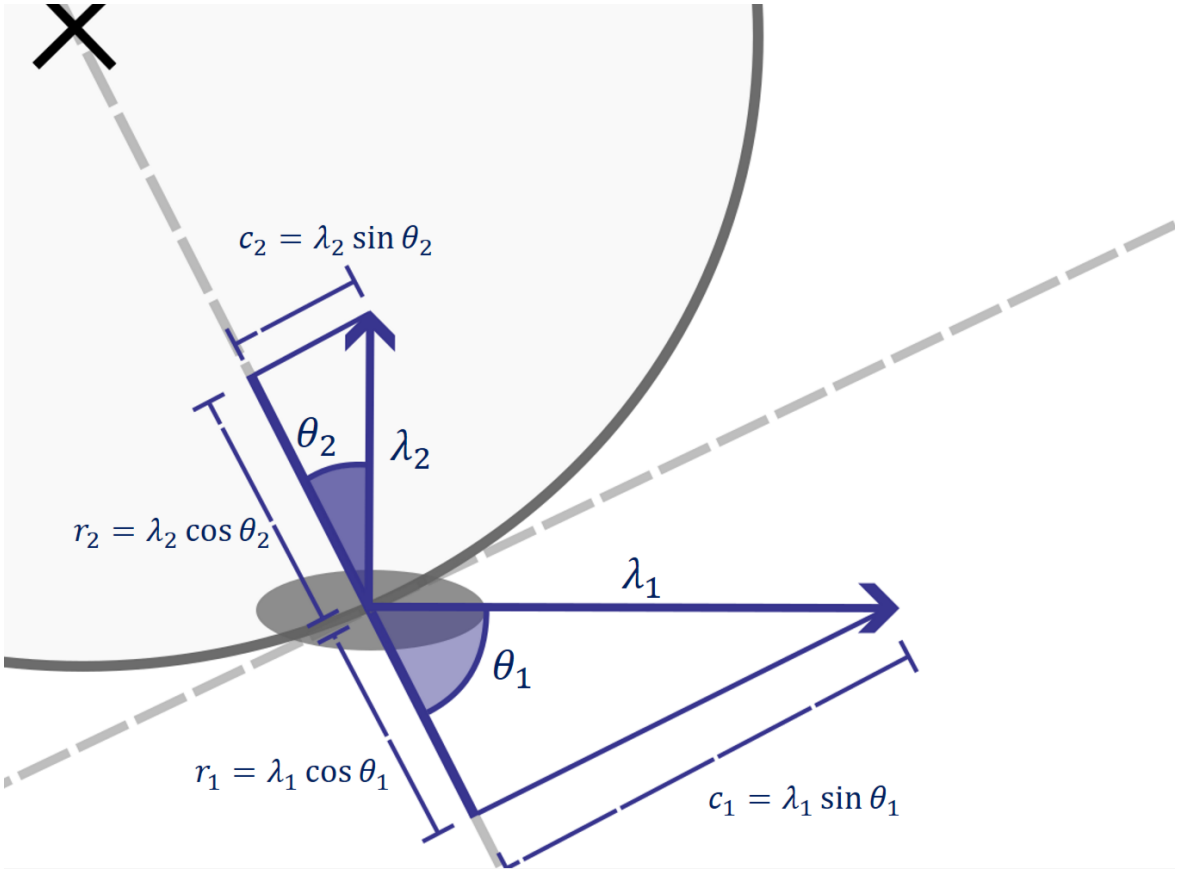

Figure 3.6: The eigenvectors represented by the ellipse in Figure 3.5 in the same coordinate system. Radial and circumferential components r_i and c_i are defined by corresponding θ_i and λ_i.

rate curves as seen in (**theory section**). Whether we get a positive or negative peak depends on the sums of positive and negative eigenvalues λ_i modulated by the trigonometric functions defined by strain rate angles θ_i.

To get correct peak values, we need to make sure that the units are scaled correctly throughout the calculation process. Firstly, we need to keep count of the amount of tensors generated in the LV at any frame as the myocardium mask changes shape throughout the cardiac cycle. Dividing the strain rate sum for this frame by this amount is how we get a weighted average measurement and also prevent larger LV cross-sections from giving 'more' signal because it has more voxels in the mask. Secondly, the units of the velocity components are cm/s, and we want strain rate measured in the unit s^{-1} which means all spatial and temporal variables should be converted to cm and s.

Previously, we have smoothed the velocity field in the SHAX xy-plane, but we have not yet smoothed our data in the time dimension. We expect the initial curves to be noisy because of this. To solve this we simply apply a running average smoothing function on the strain rate curves. The running average function convolves the curve with a kernel of length $N = 2,4,6...$ with elements $1/N$. For $N = 4$ a datapoint is transformed to the average of itself and its 4 surrounding points within the kernel.

Figure 3.7 shows a simple example of the smoothing application of the running average

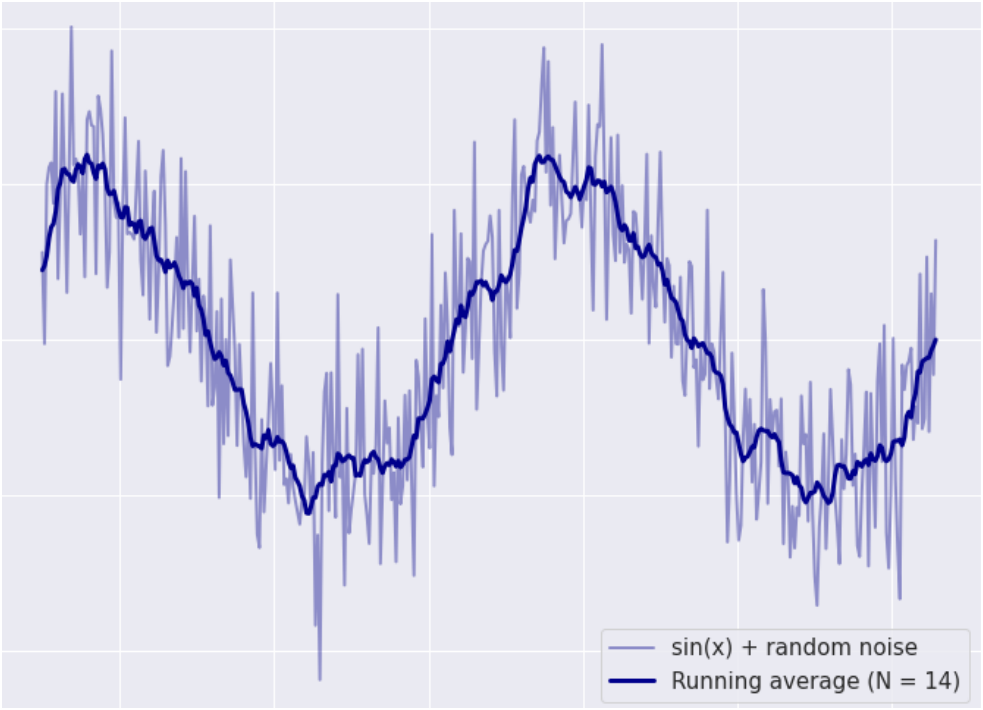

Figure 3.7: Sine signal with random noise and a curve showing the same signal smoothed by running average function using $N = 14$.

function on a noisy sine wave. In this example we see that the 'underlying' sine curve becomes clearer and has more distinct peaks and valleys, but it is also worth noting that this function also essentially acts as a low-pass filter on the signal. This means that the highest signal peaks are reduced after smoothing, and keep in mind that higher kernel sizes N give both more smoothing and lower peaks. To minimize the chance of reducing the peak values of our 'underlying' signal, we will attempt to find a balance by finding the lowest N that gives readable and coherent curves with distinct peaks.

3.3.6 Global LV strain

From theory section (...) we know that we can find strain from time-integrating strain rate. In our framework we use cumulative trapezoidal numerical integration to produce strain curves from our strain rate curves. Specifically, we use the `"cumtrapz"` function from the SciPy module. The units will be %, representing relative deformation from the initial time-point.

Despite previously smoothing the strain rate data, the strain curves will still be affected by background noise which accumulates during integration. The effect of this is that the strain curve values become increasingly distorted by the accumulated noise toward the end of the cardiac cycle. We can work around this based on assuming that the strain curves are cyclic from the initial time-point to end-diastole.

When integrating, we set the initial value to 0. The strain value we find at end diastole will likely not have returned to around zero due to the noise, but we do some subtle changes to force this boundary condition. Firstly, we produce two strain curves; one

that is integrated forward in time and one the other way. The weighted average sum of these two functions should now be affected by noise equally at the beginning and end of the cardiac cycle (27).

Secondly, we apply a weighting function that equals to 1 for the majority of the duration, but cuts off to 0 toward the beginning and end of the cardiac cycle. This step is mostly for creating a cleaner visual, and gives us strain curves that look cyclic by starting and stopping at 0 without affecting the peak values.

3.3.7 Regional strain and strain rate

To perform regional strain and strain rate analysis, we want to divide the LV into sections that can be analyzed separately to assess strain homogeneity. From the TPM data structure we can find time-dependent sector maps with the same dimensions as the image and velocity matrices that assign every voxel to one of 36 sectors as shown in Figure 3.8A. Infarcted hearts will also include infarct sectors in the metadata designed during processing. In the case of the figure, the metadata would contain a tuple "$(1, 10)$" representing an infarct sector range from 1 to 10.

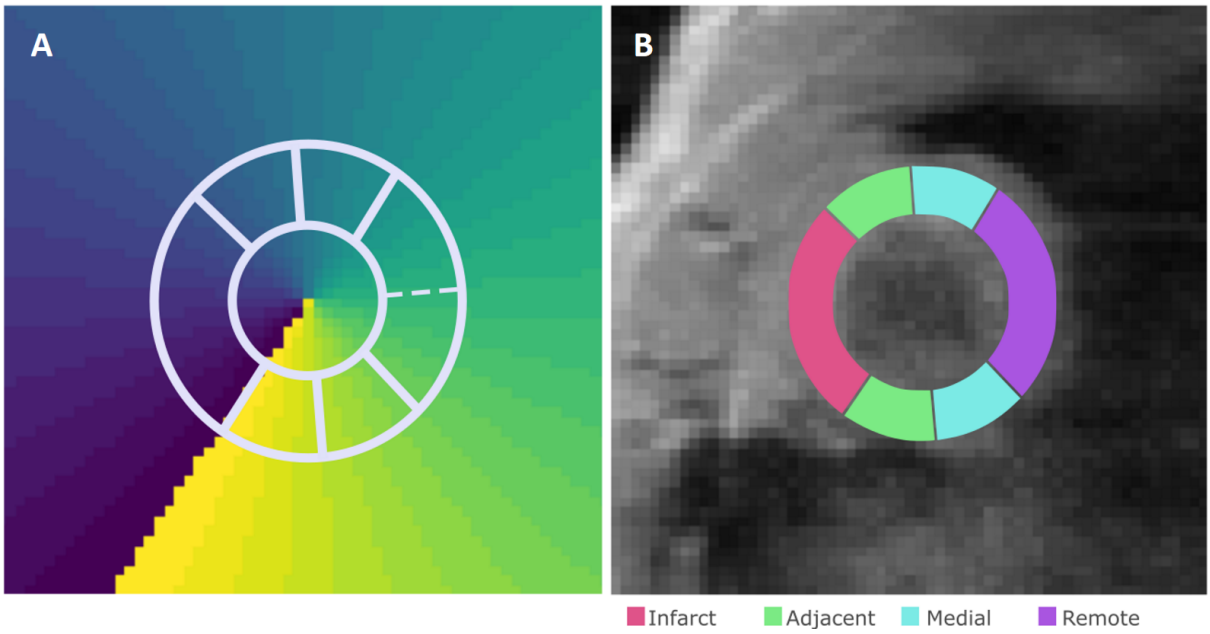

*Figure 3.8: **A**: Sector map plotted as a clockwise color scale from sector 1 to 36, divided by isotropic lines from the LV center. Different LV sections are outlined where the largest (from sector 1 to 10) represents the infarct sectors of this heart. The rest is divided into 6 equal parts. **B**: The same sector groups color coded based on infarct proximity.*

For the infarcted hearts, we want the infarcted sectors (as determined by the metadata) to be part of one group. The remaining LV will be split into six and distributed to three groups based on proximity to the infarct sectors: adjacent, medial, remote (5). This is shown in Figure 3.8B. If the remaining sector amount is not divisible by 6 we round down to the closest number and assign the remaining sectors to the remote group.

(cut?) A unique issue happens when both sector 1 and 36 are in a group we are checking

for viable voxels, which is very likely. This means that this sequence will have a reverse range like for example $[32, 6]$, which Python struggles to interpret. A simple trick to solve this is to also check if the voxel is *not* in the range $[6, 32]$. (are python syntax issues relevant?)

The Sham control group will of course not have infarct sectors, and some in the MI group as well if there was no visible infarct in the MRI LGE images (mention LGE in theory/data overview?). In these cases, we choose an infarct sector range approximately where we find infarction in the MI hearts and rename the groups to "Group 1" and so on. For this use we have chosen to define Group 1 by the range $[4, 13]$ which ensures that the four groups approximately cover the same amount of sectors.

We can now perform strain and strain rate analyses like we did for the whole LV with each of these groups, which lets us observe regional variation between different sections of the LV.

3.3.8 Eigenvector angle distributions

The analysis described thus far relies on the vector decomposition of strain rate tensor eigenvectors and eigenvalues in the radial and circumferential direction in our LV model, which is conventional in LV strain analysis. However, a unique property of our tensor framework is that we can look at distributions containing tensor data for every individual voxel instead of just the integrated total strain rate of a frame.

We will attempt to make use of this by plotting distributions of eigenvector angles in the range $\theta_i \in [0,\ 90]^\circ$ over the cardiac cycle duration. We will divide the vectors into two groups based on whether they describe stretch or compression. The intent with this kind of analysis is to study how the myocardium is organized as it deforms during the cardiac cycle, regardless of the magnitude of strain rate and unrestrained by conventional LV geometry, and see if angle distribution characteristics correlate to infarct progression.

To the extent of our knowledge, this kind of analysis has not been performed before to assess heart function. This means that we need to observe these distributions for sham and MI hearts and attempt to interpret them and see if there are quantifiable differences we can establish as a parameter that reflects myocardial function. This will be discussed in section 3.4 in the context of statistical analysis.

3.3.9 Framework adjustments for 3D analysis

We can expand our framework to include 3D strain rate tensors, which lets us perform strain analysis out of the SHAX xy-plane. This requires the introduction of the longitudinal axis and another directional parameter ϕ, as defined in Figure 3.9. We choose a cylindrical coordinate system in our 3D model, meaning that we define the longitudinal direction to always be in the z-direction and that the LV center is always defined in-plane for any slice along the LV.

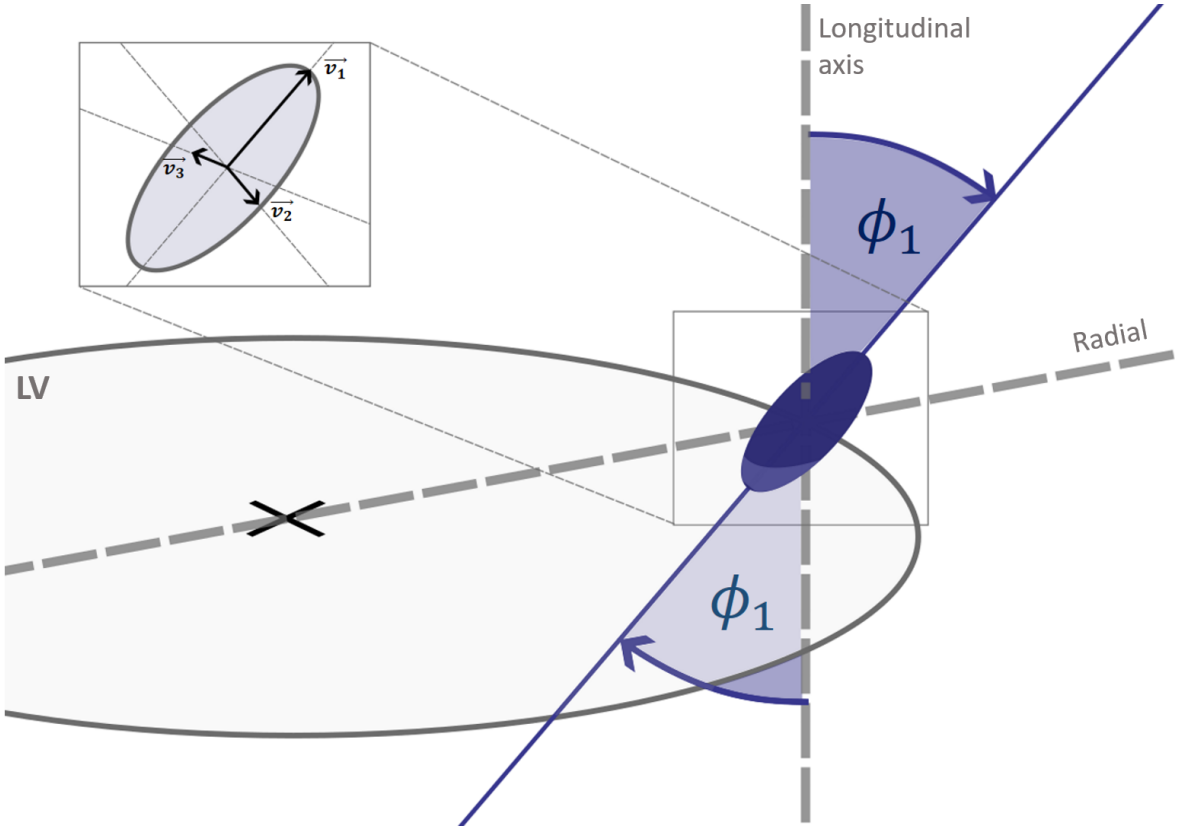

Figure 3.9: 3D strain rate tensor ellipsoid placed in LV coordinate system, where its most positive eigenvector $\vec{v}_1$ has an angle ϕ_1 relative to the longitudinal axis.

The depicted ellipsoid is spanned by three orthogonal eigenvector and eigenvalue pairs as established in Theory section 2.4 that can point in any directions in 3D space, unlike the 2D tensors confined in the xy-space. We choose to describe these directions using $(\theta,\ \phi)$-coordinates, where θ relative to radial axis is defined like before and is found from in-plane projections of each eigenvector.

The in-plane angle θ can be used like before to obtain radial and circumferential components of strain rate, but now we can also find the longitudinal component simply as $l_i = \lambda_i cos\phi_i$. When using 3D tensors, the framework will also collect directional parameters with ϕ values in the range $\phi \in [0,\ 90]^\circ$ to study how the distributions change over the cardiac cycle, where $\phi = 0^\circ$ is completely out-of-plane and $\phi = 90^\circ$ is completely in-plane.

(apical/basal management?)

3.4 Statistical analysis

(short recap, 2d 3d framework and segmentation models)

To study the infarct progression of the rat hearts, we will apply our Python framework to analyse the entire study population and collect characteristic curve parameters that represent myocardial function and see how these change over days after operation. We

will divide Sham and MI hearts into respective groups, with Sham acting as control group, and compare them.

The point of the comparison and statistical analysis is to see if the infarcted hearts show trends over time that deviate from the control group, and could indicate the effects of infarct progression. Based on previous studies, we expect to see reduction of strain and strain rate peak values over time in the MI hearts (cite). (((We also expect to see an increase in dyssynchrony in the basal slice segmentation model, defined as the standard deviation between the time points of the regional strain peaks (cite).)))

(new parameters; establish these here, hint at the results)

(Linear fits of grouped Sham and MI measurements will present a visual the estimate of change within the groups, where the slope for the Sham fit is a baseline for comparison.)

(list explicitly the questions we wish to ask using 2d tensor analysis)

The parameters we will collect from the 2D strain rate tensor analysis are:

Condition - (1 = MI, 0 = Sham)

Time [days] - Time after operation

GRS [%] - Global Radial Strain peak

GCS [%] - Global Circumferential Strain peak

GRSRs [s^{-1}] - Systolic Global Radial Strain Rate peak

GRSRd [s^{-1}] - Diastolic Global Radial Strain Rate peak

GCSRs [s^{-1}] - Systolic Global Circumferential Strain Rate peak

GCSRd [s^{-1}] - Diastolic Global Circumferential Strain Rate peak

RSDI [%] - Radial Strain Delay Index

CSDI [%] - Circumferential Strain Delay Index

Stretch Angle Peak [°]

Stretch Angle Minima [°]

Compression Angle Peak [°]

Compression Angle Minima [°],

where the "SDI" values are defined as the standard deviation of the strain curve peak times of the different LV regions as a percentage of the cardiac cycle duration, to com-

pensate for rats having different heart rates (26). Higher values represent a higher level of dyssynchrony in the LV. The angle distribution parameter definitions are original, but it is reasonable to expect the strain rate direction to have distinct peaks during systole and diastole from what we know from (*theory section on LV strain rate*). (comment on using a single strain rate peak in diastole instead of two?)

For analysis using 3D strain rate tensors (list explicitly the questions we wish to ask using 3d tensor analysis/segmentation model/apical and basal variation), additional parameters will be collected:

GLS [%] - Global Longitudinal Strain peak

GLSRs [s^{-1}] - Systolic Global Longitudinal Strain Rate peak

GLSRd [s^{-1}] - Diastolic Global Longitudinal Strain Rate peak

phi [°] - ,

where "global" in this case refers to all LV slices used.

We will use the Pandas module in a Python script to organize the parameters measured during analysis for each dataset. The scipy "stats" module contains functions that allow us to calculate (pearsson, t-test). Independent two sample T-tests will be performed to estimate statistical significant difference between the Sham and MI groups.

Specifically, we will use these tests at

(pearson correlation, null hypothethis)

('Er fravær av signifikans på forskjell mellom to grupper det samme som signifikant likhet mellom gruppene?')

(type 1 and type 2 errors)

(confidence interval, 95 percentile)

(assuming linear regression is just an assumption, but could provide useful info nonetheless. for small data samples, a simpler model may be more appropriate.)

(some parameters were determined after seeing results/plots. should these be mentioned here?)

Chapter 4

Results

This chapter presents the results produced by our Python framework. We have produced plots of strain rate, strain, and eigenvector angle distributions from the cardiac cycles of Sham and MI rat hearts. We have collected curve parameters that were used in statistical analysis to attempt to detect reduction in myocardial function and link it to MI progression. We separate the results using 2D and 3D strain rate tensors in respective sections due to...

4.1 2D strain rate tensor analysis

Results in this section were acquired from analyzing in-plane motion in a single basal LV slice using 2D strain rate tensors.

4.1.1 Visualization

Figure 4.1 demonstrates the ellipse plot framework in action in two different time points, showing 2D strain rate tensors represented within the mask. The ellipse opacity corresponds to the invariant $I = \lambda_1^2 + \lambda_2^2$ from Equation 2.4. Every other voxel is sampled in this case, or in other words: they are sampled in a grid with spacing of one voxel for the sake of visibility. For quantitative results, however, we always utilize all viable voxels within the myocardium.

We have also used our ellipse plotting tool to visually evaluate the effectiveness of the velocity smoothing function (Equation 3.1) by looking for border artifacts in plots with tensors sampled in all masked voxels. Equivalent plots using eroded masks were also produced for the sake of comparison. This is demonstrated in Figure (appendix?).

4.1.2 Global strain rate

4.1.3 Global strain

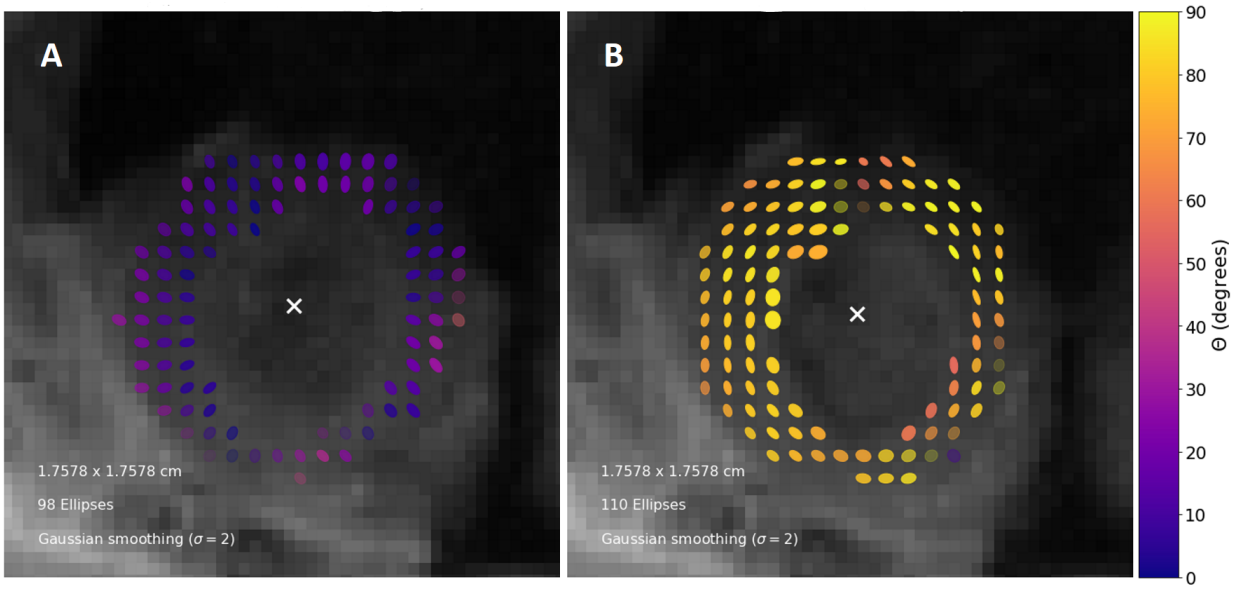

*Figure 4.1: Ellipse plots with color scale defined by direction of stretch relative to the radial direction from the heart center (marked 'X'). **A**: Mid systole, with the myocardium experiencing stretching in the radial direction and compression in the circumferential direction. **B**: Early diastole, stretch along the circumferential direction and compression in the radial.*

4.1.4 Regional strain

Figure 4.2 shows examples of ellipse and strain plots where the LV has been divided into groups to look at regional variation. Peak values on the strain curves that are collected for later statistical analysis are marked.

4.1.5 Eigenvector angle distribution

4.1.6 Progression / statistical analysis

4.2 3D strain rate tensor analysis

The results in this section were acquired from analyzing 3D motion in multiple slices covering most of the LV using 3D strain rate tensors. (...)

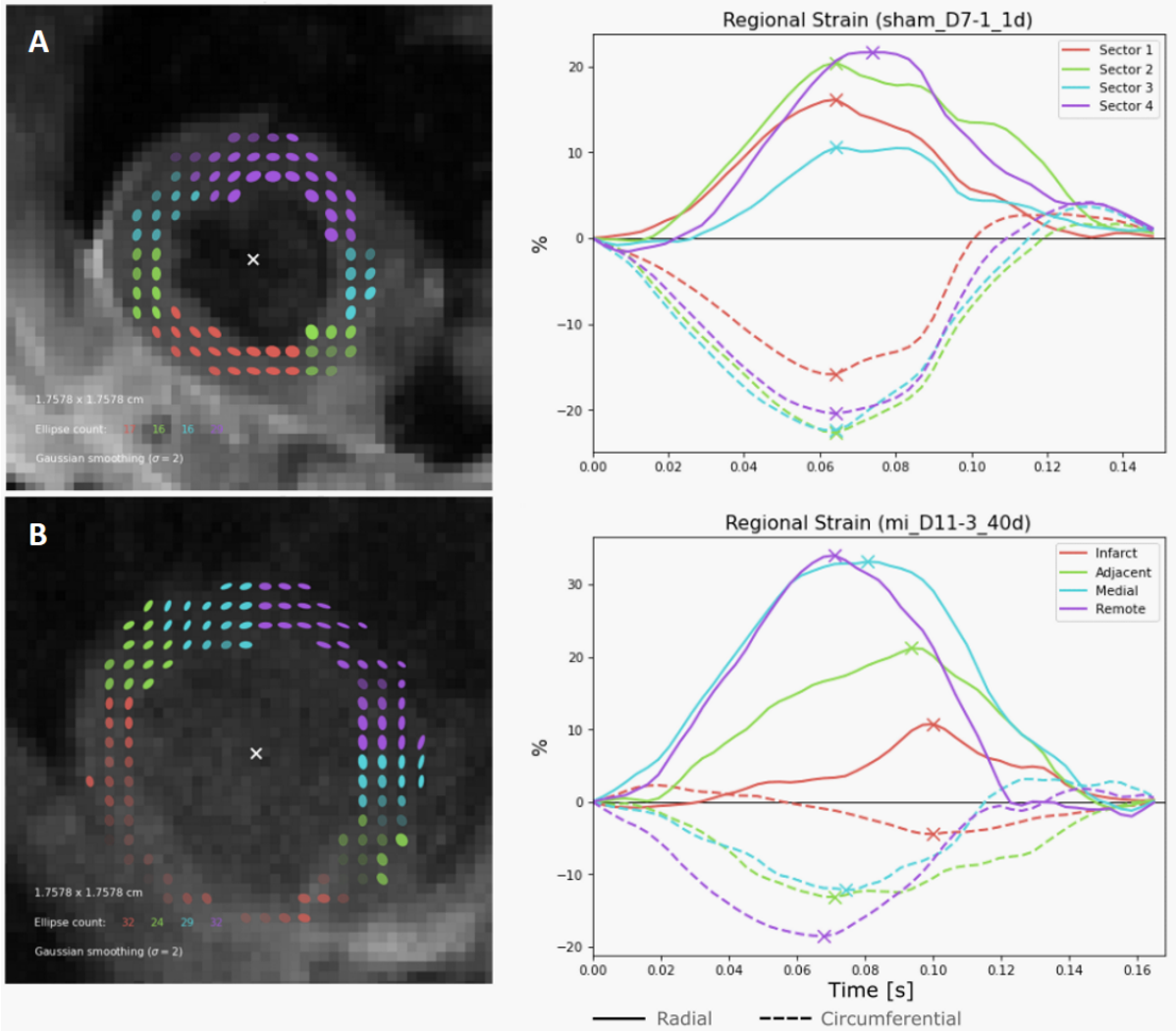

Figure 4.2: Regional strain analysis of a Sham and MI heart, featuring strain rate tensor ellipse plots at early diastole and strain plots with color coding based on group. ***A****: Sham heart with arbitrary, numerated sectors.* ***B****: MI heart 40 days after infarction, groups based on infarct sector and proximity.*

Chapter 5

Discussion

The aim of this thesis was to ...

Strain and strain rate curve peak values in the radial, circumferential and longitudinal directions will be compared to literature to assess the viability of the Selskog method for quantitative analysis.

5.1 Tensor Visualization

As seen in Figure 4.1 our framework produces ellipse plots that visualize strain rate tensors in the LV comparable to literature (14). During systole, the plot shows expansion in the radial direction and compression in the circumferential. In the diastole frame we see the opposite.

The plots also map ellipse color based on the direction of stretch, or the most positive eigenvalue. Even though the direction of strain rate appears relatively homogenic across the myocardium at these frames, we can also see some variation. The distribution of strain rate directions will be discussed further in Section xx.

In Figure 4.2 we display an alternative color scheme that distinguishes between the different LV groups used for regional analysis. Here, we also see clearly the reduced total strain rate in the MI heart infarction sector from the reduced ellipse opacity. The highest strain rate values appear in the remote group in the MI heart which is visualized by ellipses that appear more "squeezed". This could be the effect of remodelling.

Our strain rate tensor visualization framework appears to produce ellipse plots with the intended effects.

5.2 Global strain rate

Chapter 6

Conclusion

Bibliography

[1] J. G. Cleland, K. Swedberg, F. Follath, M. Komajda, A. Cohen-Solal, J. C. Aguilar, R. Dietz, A. Gavazzi, R. Hobbs, J. Korewicki, H. C. Madeira, V. S. Moiseyev, I. Preda, W. H. van Gilst, J. Widimsky, N. Freemantle, J. Eastaugh, and J. Mason. The euroheart failure survey programme– a survey on the quality of care among patients with heart failure in europe. part 1: patient characteristics and diagnosis. *Eur Heart J*, 24(5):442–63, 2003. (document)

[2] F. Valente, L. Gutierrez, L. Rodriguez-Eyras, R. Fernandez, M. Montano, A. Sao-Aviles, V. Pineda, A. Guala, H. Cuellar, A. Evangelista, and J. Rodriguez-Palomares. Cardiac magnetic resonance longitudinal strain analysis in acute st-segment elevation myocardial infarction: A comparison with speckle-tracking echocardiography. *Int J Cardiol Heart Vasc*, 29:100560, 2020. (document)

[3] P. Selskog, E. Heiberg, T. Ebbers, L. Wigström, and M. Karlsson. Kinematics of the heart: strain-rate imaging from time-resolved three-dimensional phase contrast mri. *IEEE Trans Med Imaging*, 21(9):1105–9, 2002. (document), 2.4, 3.3.1, 3.3.2

[4] C. Mátyás, A. Kovács, B. T. Németh, A. Oláh, S. Braun, M. Tokodi, B. A. Barta, K. Benke, M. Ruppert, B. K. Lakatos, B. Merkely, and T. Radovits. Comparison of speckle-tracking echocardiography with invasive hemodynamics for the detection of characteristic cardiac dysfunction in type-1 and type-2 diabetic rat models. *Cardiovasc Diabetol*, 17(1):13, 2018. (document)

[5] T. Røe Å, M. Ruud, E. K. Espe, O. Manfra, S. Longobardi, J. M. Aronsen, E. S. Nordén, T. Husebye, T. R. S. Kolstad, A. Cataliotti, G. Christensen, O. M. Sejersted, S. A. Niederer, GØ Andersen, I. Sjaastad, and W. E. Louch. Regional diastolic dysfunction in post-infarction heart failure: role of local mechanical load and serca expression. *Cardiovasc Res*, 115(4):752–764, 2019. (document), 3.3.7

[6] I. Johansson, P. Joseph, K. Balasubramanian, J. J. V. McMurray, L. H. Lund, J. A. Ezekowitz, D. Kamath, K. Alhabib, A. Bayes-Genis, A. Budaj, A. L. L. Dans, A. Dzudie, J. L. Probstfield, K. A. A. Fox, K. M. Karaye, A. Makubi, B. Fukakusa, K. Teo, A. Temizhan, T. Wittlinger, A. P. Maggioni, F. Lanas, P. Lopez-Jaramillo, J. Silva-Cardoso, K. Sliwa, H. Dokainish, A. Grinvalds, T. McCready, S. Yusuf, and G. Chf Investigators. Health-related quality of life and mortality in heart failure: The global congestive heart failure study of 23 000 patients from 40 countries. *Circulation*, 143(22):2129–2142, 2021. 1

[7] S. Heo, T. A. Lennie, C. Okoli, and D. K. Moser. Quality of life in patients with heart failure: ask the patients. *Heart Lung*, 38(2):100–8, 2009. 1

[8] NIH NHLBI. What is Heart Failure? Last updated March 2022. https://www.nhlbi.nih.gov/health/heart-failure. 1

[9] A. Scatteia, A. Baritussio, and C. Bucciarelli-Ducci. Strain imaging using cardiac magnetic resonance. *Heart Fail Rev*, 22(4):465–476, 2017. 1

[10] P. Lim, A. Buakhamsri, Z. B. Popovic, N. L. Greenberg, D. Patel, J. D. Thomas, and R. A. Grimm. Longitudinal strain delay index by speckle tracking imaging: a new marker of response to cardiac resynchronization therapy. *Circulation*, 118(11):1130–7, 2008. 1

[11] M. J. Gotte, T. Germans, I. K. Russel, J. J. Zwanenburg, J. T. Marcus, A. C. van Rossum, and D. J. van Veldhuisen. Myocardial strain and torsion quantified by cardiovascular magnetic resonance tissue tagging: studies in normal and impaired left ventricular function. *J Am Coll Cardiol*, 48(10):2002–11, 2006. 1

[12] G. Pedrizzetti, P. Claus, P. J. Kilner, and E. Nagel. Principles of cardiovascular magnetic resonance feature tracking and echocardiographic speckle tracking for informed clinical use. *J Cardiovasc Magn Reson*, 18(1):51, 2016. 1

[13] A. Bjørnerud and E. K. Espe. *Physics of MR imaging: Compendium for FYS4740/9740*. 2023. 2.1

[14] H. Haraldsson, L. Wigstrom, M. Lundberg, A. F. Bolger, J. Engvall, T. Ebbers, and J. P. Kvitting. Improved estimation and visualization of two-dimensional myocardial strain rate using mr velocity mapping. *J Magn Reson Imaging*, 28(3):604–11, 2008. 3.3.3, 5.1

[15] V. M. Almaas, K. H. Haugaa, E. H. Strom, H. Scott, H. J. Smith, C. P. Dahl, O. R. Geiran, K. Endresen, S. Aakhus, J. P. Amlie, and T. Edvardsen. Noninvasive assessment of myocardial fibrosis in patients with obstructive hypertrophic cardiomyopathy. *Heart*, 100(8):631–8, 2014.

[16] M. S. Amzulescu, M. De Craene, H. Langet, A. Pasquet, D. Vancraeynest, A. C. Pouleur, J. L. Vanoverschelde, and B. L. Gerber. Myocardial strain imaging: review of general principles, validation, and sources of discrepancies. *Eur Heart J Cardiovasc Imaging*, 20(6):605–619, 2019.

[17] B. A. Bendiksen, G. McGinley, I. Sjaastad, L. Zhang, and E. K. S. Espe. A 4d continuous representation of myocardial velocity fields from tissue phase mapping magnetic resonance imaging. *PLoS One*, 16(3):e0247826, 2021.

[18] X. Chen, J. Pan, J. Shu, X. Zhang, L. Ye, L. Chen, Y. Hu, and R. Yu. Prognostic value of regional strain by cardiovascular magnetic resonance feature tracking in hypertrophic cardiomyopathy. *Quant Imaging Med Surg*, 12(1):627–641, 2022.

[19] X. Chen, J. Pan, J. Shu, X. Zhang, L. Ye, L. Chen, Y. Hu, and R. Yu. Prognostic value of regional strain by cardiovascular magnetic resonance feature tracking in hypertrophic cardiomyopathy. *Quant Imaging Med Surg*, 12(1):627–641, 2022.

[20] N. D'Elia, J. D'Hooge, and T. H. Marwick. Association between myocardial mechanics and ischemic lv remodeling. *JACC Cardiovasc Imaging*, 8(12):1430–1443, 2015.

[21] E. K. Espe, J. M. Aronsen, K. Skardal, J. E. Schneider, L. Zhang, and I. Sjaastad. Novel insight into the detailed myocardial motion and deformation of the rodent heart using high-resolution phase contrast cardiovascular magnetic resonance. *J Cardiovasc Magn Reson*, 15(1):82, 2013. 3.1.2

[22] E. K. Espe, J. M. Aronsen, B. Skrbic, V. M. Skulberg, J. E. Schneider, O. M. Sejersted, L. Zhang, and I. Sjaastad. Improved mr phase-contrast velocimetry using a novel nine-point balanced motion-encoding scheme with increased robustness to eddy current effects. *Magn Reson Med*, 69(1):48–61, 2013. 3.1.2

[23] E. K. S. Espe, J. M. Aronsen, M. Eriksen, O. M. Sejersted, L. Zhang, and I. Sjaastad. Regional dysfunction after myocardial infarction in rats. *Circ Cardiovasc Imaging*, 10(9), 2017. 3.1

[24] N. Funabashi, H. Takaoka, K. Ozawa, T. Kamata, M. Uehara, I. Komuro, and Y. Kobayashi. Quantitative differentiation of lv myocardium with and without layer-specific fibrosis using mri in hypertrophic cardiomyopathy and layer-specific strain tte analysis. *Int Heart J*, 59(3):523–530, 2018. 3.3.2

[25] J. J. Hjertaas, E. Einarsen, E. Gerdts, M. Kokorina, C. A. Moen, S. Urheim, S. Saeed, and K. Matre. Impact of aortic valve stenosis on myocardial deformation in different left ventricular levels: A three-dimensional speckle tracking echocardiography study. *Echocardiography*, 40(10):1028–1039, 2023.

[26] Ahmed M. El Missiri. Echocardiographic assessment of left ventricular mechanical dyssynchrony a practical approach. *Echocardiography*, 2014. 3.4

[27] N. J. Pelc, M. Drangova, L. R. Pelc, Y. Zhu, D. C. Noll, B. S. Bowman, and R. J. Herfkens. Tracking of cyclic motion with phase-contrast cine mr velocity data. *J Magn Reson Imaging*, 5(3):339–45, 1995. 3.3.6

[28] M. Ruppert, B. K. Lakatos, S. Braun, M. Tokodi, C. Karime, A. Olah, A. A. Sayour, I. Hizoh, B. A. Barta, B. Merkely, A. Kovacs, and T. Radovits. Longitudinal strain reflects ventriculoarterial coupling rather than mere contractility in rat models of hemodynamic overload-induced heart failure. *J Am Soc Echocardiogr*, 33(10):1264–1275 e4, 2020.

[29] T. J. Samuel, A. P. Oneglia, D. J. Cipher, J. A. Ezekowitz, J. R. B. Dyck, T. Anderson, J. G. Howlett, D. I. Paterson, R. B. Thompson, and M. D. Nelson. Integration of longitudinal and circumferential strain predicts volumetric change across the cardiac cycle and differentiates patients along the heart failure continuum. *J Cardiovasc Magn Reson*, 25(1):55, 2023.

[30] R. Tanacli, D. Hashemi, T. Lapinskas, F. Edelmann, R. Gebker, G. Pedrizzetti, A. Schuster, E. Nagel, B. Pieske, H. D. Düngen, and S. Kelle. Range variability in cmr feature tracking multilayer strain across different stages of heart failure. *Sci Rep*, 9(1):16478, 2019.

Appendix A